

# Admittance-Based Controller Design for Physical Human-Robot Interaction in the Constrained Task Space

Wei He, *Senior Member, IEEE*, Chengqian Xue, Xinbo Yu, *Student Member, IEEE*, Zhijun Li, *Senior Member, IEEE*, Chenguang Yang, *Senior Member, IEEE*

**Abstract**— In this paper, an admittance-based controller for physical human-robot interaction (pHRI) is presented for to perform coordinated operation in the constrained task space. An admittance model and a soft saturation function are employed to generate a differentiable reference trajectory to ensure that the end-effector motion of the manipulator complies with human operation and avoids collision with surroundings. Then an adaptive neural network (NN) controller involving integral barrier Lyapunov function (IBLF) is designed to deal with tracking issues. Meanwhile, the controller can guarantee the end-effector of the manipulator limited in the constrained task space. A learning method based on radial basis function neural network (RBFNN) is involved in controller design to compensate for dynamics uncertainties and improve tracking performance. IBLF method is provided to prevent violations of the constrained task space. We prove that all states of the closed-loop system are semi-globally uniformly ultimately bounded (SGUUB) by utilizing Lyapunov stability principles. At last, the effectiveness of the proposed algorithm is verified on a Baxter robot experiment platform.

**Note to Practitioners**— This work is motivated by the neglect of safety in existing controller design in pHRI, which exists in industry and services, such as assembly, medical care, etc. It is considerably required in controller design for rigorously handling constraints. Therefore in this paper, we propose a novel admittance-based human-robot interaction controller. The developed controller has the following functionalities: 1) Ensuring reference

trajectory remaining in the constrained task space: a differentiable reference trajectory is shaped by the desired admittance model and a soft saturation function; 2) Solving uncertainties of robotic dynamics: a learning approach based on RBFNN is involved in controller design; 3) Ensuring the end-effector of the manipulator remaining in the constrained task space: different from other barrier Lyapunov function (BLF), IBLF is proposed to constrain system output directly rather than tracking error, which may be more convenient for controller designers. The controller can be potentially applied in many areas: 1) it can be used in the rehabilitation robot to avoid injuring the patient by limiting the motion; 2) it can ensure the end effector of the industrial manipulator in a prescribed task region. In some industrial tasks, dangerous or damageable tools are mounted on the end-effector, and it will hurt human and bring damage to the robot when the end-effector is out of the prescribed task region; 3) it may bring a new idea to design controller for avoiding collisions in pHRI when collisions occur in the prescribed trajectory of end-effector.

**Index Terms**—Adaptive neural network control, physical human-robot interaction (pHRI), admittance control, integral barrier Lyapunov function (IBLF), motion constraint.

## I. INTRODUCTION

In recent years, as robots transition from industrial applications to service areas, social robots become more and more significant in our daily life [1]–[6]. In view of security of pHRI, the significance of methods for interaction control is increasing [7]–[10]. Control design in pHRI tasks is much more complicated than that in non-interactive scenarios. Such as rehabilitation robots, they should not only guide motion of patient limb but also comply with forces exerted by patient for compliance. Only the motion control method may not meet requirements for complex tasks in pHRI.

Considering a classical pHRI scenario as in Fig. 1, *human* and *robot* perform coordinated operation in the constrained task space. *Robot* can be a rehabilitation robot or an industrial manipulator, and *human* operates the end-effector of *robot* for recovering in rehabilitation or performing some tasks collaboratively. The main difficulty in such tasks lies in controlling manipulator complying with operator and constraining it in the predefined task space simultaneously. In order to solve issues of compliance in pHRI, various control methods have been

This work has been supported in part by the National Natural Science Foundation of China under Grant 61933001 and 61873298, in part by the Fundamental Research Funds for the China Central Universities of USTB under Grant FRF-TP-19-001C2, in part by the Joint Funds of Equipment Pre-Research and Ministry of Education of China under Grant 6141A02033339, and in part by the Beijing Top Discipline for Artificial Intelligence Science and Engineering, University of Science and Technology Beijing.

W. He, C. Xue and X. Yu are with Institute of Artificial Intelligence, University of Science and Technology Beijing, Beijing 100083, China, and also with Key Laboratory of Knowledge Automation for Industrial Processes of Ministry of Education, School of Automation and Electrical Engineering, University of Science and Technology Beijing, Beijing 100083, China. Corresponding author is W. He. (Email: weihe@ieee.org)

Z. Li is with the Department of Automation, University of Science and Technology of China, Hefei 230026, China.

C. Yang is with the Bristol Robotics Laboratory, University of the West of England, Bristol, BS16 1QY, U.K.

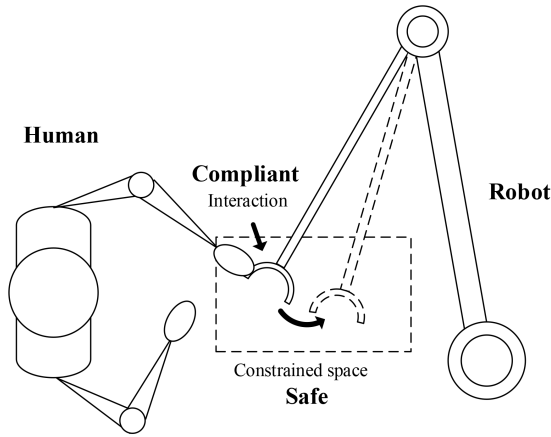


Fig. 1: A typical human-robot interactive scenario in the constrained task space.

proposed. In [11], hybrid position/force control is proposed firstly to achieve compliant interaction by controlling terminal position and contact force simultaneously. Then some studies have made extensions to this control scheme for solving pHRI problems [12]–[14]. In [15], impedance control is proposed firstly by Hogan to express the relationships between contact force and state in a prescribed impedance model. Compared with hybrid force/position control, impedance control does not require control transitions between contact and non-contact situations and has the better performance in robustness. Depending on the causality of the controller, there are two ways to implement impedance control, which are often referred as *impedance control* and *admittance control* in literature [16]. In recent years, impedance control and admittance control have become two of the most efficient control methods in pHRI [17]–[19]. In [20], an adaptive admittance control is proposed to enable human interacting with robot whose behavior likes a prescribed admittance model under control design. In [21], an adaptive admittance control method without external sensors is proposed to enable pHRI for manipulators in the industrial environment. In [22], a learning impedance controller is proposed to control robotic system following a given impedance model and achieve interactive control objective for pHRI. In [23], a unified torque-impedance controller is proposed for the pneumatically actuated antagonistic manipulator joint. The controller has good performance for both operations of trajectory tracking and torque control and can handle the contact loss fast and accurately in pHRI. In [24], a hybrid passivity-based cartesian force/impedance controller is proposed for robots to realize the accurate force tracking, handle unexpected contact loss and avoid chattering behavior. Although admittance control can improve the performance in pHRI, such method does not guarantee operational security since admittance control can only regulate interactive force without constraining the position of manipulators. Emphatically, a major obstacle in the field of application is that position constraints are not considered in the above design. Therefore, position constraints should be considered in the control design to ensure security during pHRI, .

Due to actual physical device limitations [25]–[28], system

performance and safety requirements [29]–[32], output or states in most systems should be constrained in practice [33]–[37]. Therefore, it is considerably significant to maintain system's outputs in desired constraints [38]–[41]. For a nonlinear system of manipulators, output constraints can be regarded as position constraints. In recent years, BLF is proposed for solving output constrained issues in complex systems [42]. In [43], an asymmetric time-varying BLF is employed in strict feedback nonlinear systems to ensure the time-varying output constraints. In [44], an adaptive control scheme is developed for nonlinear stochastic systems with unknown parameters. All the states of the systems are required to be constrained in bounded compact sets with *log*-type BLF. In [45], the output constraint problem of uncertain nonstrict-feedback systems is handled by utilizing a BLF. In [46], *tan*-type BLF is used to maintain output in constraints under systematic control design for strict-feedback nonlinear systems. In [47], *tan*-type BLF is incorporated with a novel fault-tolerant leader-follower formation control scheme to ensure the angle constraints. Compared with the conventional *log*-type BLF and *tan*-type BLF, controllers with a novel IBLF can constrain state signals directly, rather than error signals [48]. From the engineering point of view, the initial states of robots can be relaxed to the whole constrained space. Therefore, in this paper, IBLF is used to guarantee the end-effector of the manipulator in the constrained task space.

The uncertainty of manipulator dynamics cannot be ignored in robot controller design [49]–[51]. To solve uncertainty issues, NNs are widely used to estimate unknown parameters of system in literature [52]–[55]. In [56], adaptive NNs are used to approximate uncertainties in rehabilitation robot dynamics and adapt the interactions between robot and patient. In [57], an adaptive NN control is used to research the multirate networked industrial process control problem in double-layer architectures. In [58], a fuzzy NN learning algorithm is proposed to identify the uncertain plant model and the tracking performance of the controller is guaranteed. Compared with other NN control methods [59], RBFNN performs better in approximating unknown model of a nonlinear function because it is a local approximation network with simple structure and fast convergence speed.

Based on above discussion, in this paper, an IBLF and a soft saturation function are jointly designed to guarantee the manipulator end-effector within the constrained task space in two lines: controller design and path planning. An admittance-based controller for pHRI, involving in IBLF and RBFNN learning method, is designed for solving uncertainties in dynamics. Meanwhile, the controller can guarantee the end-effector of the manipulator in the constrained task space and improve the compliance of interaction. Compared with existing works, the main contributions of this paper include:

- 1) Compared with traditional admittance control [60], a soft saturation function is employed to further shape the tracking reference trajectory which generates from the desired admittance model, and the reference trajectory will be ensured in the constrained task space;
- 2) A learning method based on RBFNN is proposed to approximate uncertainties in manipulator dynamics, and

an adaptive NN admittance controller is designed to track the reference trajectory precisely;

- 3) Compared with common BLF, such as *log*-type BLF and *tan*-type BLF [43]–[47], IBLF is used to constrain output signals directly, rather than error signals. From the engineering point of view, setting proper position constrained boundary is more effective and convenient in a pHRI scenario. When we use other BLF methods considering constraining position error, unknown time-varying human reference trajectory may generate a time-varying constrained boundary, which may be out of our desired constrained task region. Therefore, setting prescribed position constrained boundary is required in pHRI applications to guarantee the manipulator performing coordinated operation within the constrained task space.

The rest of this paper is organized as follows: In Section II, system dynamic model and preliminaries are demonstrated. In Section III, constrained space and reference trajectory are shaped and an adaptive NN admittance controller is designed. In Section IV, experiments are designed to verify the effectiveness of the proposed method. In Section V, we summarize research results.

## II. PRELIMINARIES AND PROBLEM FORMULATION

### A. Problem Formulation

A typical pHRI in the constrained task space is shown in Fig. 1. The motion of manipulator needs to comply with human motion, and excessive interaction force brings uncomfortable feelings to human. Meanwhile operational safety should be ensured to avoid unexpected collisions with surroundings out of the constrained region. Our control objective is to design a controller for the manipulator which can track the shaped virtual trajectory and can simultaneously guarantee that: (1) the end-effector of the manipulator remains in the constrained task space strictly; (2) all error signals are SGUUB which is defined in [56]; (3) desired admittance relationship of the manipulator can be achieved under our proposed controller.

### B. Dynamics Modelling of Manipulator System

The dynamics of an  $m$ -link manipulator system in the joint space can be described as [56]:

$$\mathbf{M}(\mathbf{q})\ddot{\mathbf{q}} + \mathbf{C}(\mathbf{q}, \dot{\mathbf{q}})\dot{\mathbf{q}} + \mathbf{g}(\mathbf{q}) = \boldsymbol{\tau} - \boldsymbol{\tau}_e \quad (1)$$

where  $\mathbf{M}(\mathbf{q}) \in \mathbb{R}^{m \times m}$  denotes the inertia matrix;  $\mathbf{C}(\mathbf{q}, \dot{\mathbf{q}})\dot{\mathbf{q}} \in \mathbb{R}^m$  is the Coriolis and Centripetal torque;  $\mathbf{g}(\mathbf{q}) \in \mathbb{R}^m$  denotes the gravitational torque;  $\mathbf{q}, \dot{\mathbf{q}}, \ddot{\mathbf{q}} \in \mathbb{R}^m$  denote the joint position, velocity and acceleration vector, respectively;  $\boldsymbol{\tau}_e \in \mathbb{R}^m$  denotes the interactive torque from human or contact environment, and  $\boldsymbol{\tau} \in \mathbb{R}^m$  denotes the control input to the manipulator system.

The forward kinematic function  $\Phi(\mathbf{q})$  can map joint angle  $\mathbf{q}$  to end-effector position  $\mathbf{x}$  of the manipulator system. Therefore,  $\mathbf{x} = \Phi(\mathbf{q})$  can represent the forward kinematics of the manipulator. Differentiating the forward kinematics with respect to time, we can obtain  $\dot{\mathbf{x}} = \mathbf{J}(\mathbf{q})\dot{\mathbf{q}}$ , where  $\mathbf{J}(\mathbf{q}) \in \mathbb{R}^{n \times m}$

denotes the Jacobian matrix in manipulator system. Based on inverse kinematics,  $\dot{\mathbf{q}}$ , and  $\ddot{\mathbf{q}}$  can be calculated as follows:

$$\begin{aligned} \dot{\mathbf{q}} &= \mathbf{J}^+(\mathbf{q})\dot{\mathbf{x}} \\ \ddot{\mathbf{q}} &= \dot{\mathbf{J}}^+(\mathbf{q})\dot{\mathbf{x}} + \mathbf{J}^+(\mathbf{q})\ddot{\mathbf{x}} \end{aligned} \quad (2)$$

where  $\mathbf{x} = [x_1, x_2, \dots, x_n]^T$  is the position vector of end-effector for manipulators in the task space and  $n$  is the dimension of the end-effector coordinates. We consider the manipulators with known forward kinematic function  $\Phi(\mathbf{q})$  and Jacobian matrix  $\mathbf{J}(\mathbf{q}) \in \mathbb{R}^{n \times m}$  in this paper.  $\mathbf{J}^+(\mathbf{q})$  denotes the pseudoinverse matrix of  $\mathbf{J}(\mathbf{q})$ .  $\mathbf{x}, \dot{\mathbf{x}}, \ddot{\mathbf{x}} \in \mathbb{R}^n$  are position, velocity and acceleration vectors in the task space, respectively.

Substituting (2) into (1), we can obtain the dynamics of an  $n$ -dimension manipulator system in the task space:

$$\mathbf{M}_x(\mathbf{q})\ddot{\mathbf{x}} + \mathbf{C}_x(\mathbf{q}, \dot{\mathbf{q}})\dot{\mathbf{x}} + \mathbf{g}_x(\mathbf{q}) = \mathbf{f} - \mathbf{f}_e \quad (3)$$

where  $\mathbf{M}_x(\mathbf{q}) \in \mathbb{R}^{n \times n}$ ,  $\mathbf{C}_x(\mathbf{q}, \dot{\mathbf{q}}) \in \mathbb{R}^{n \times n}$  and  $\mathbf{g}_x(\mathbf{q}) \in \mathbb{R}^n$  denote the inertia matrix, Coriolis and Centripetal matrix and gravity vector in the task space, respectively.  $\mathbf{f}_e \in \mathbb{R}^n$  denotes external force, which is 0 when there is no contact between end-effector of manipulator and human or environment, and  $\mathbf{f} \in \mathbb{R}^n$  denotes the control input to the manipulator. These matrices and vectors can be calculated as follows:

$$\begin{aligned} \mathbf{M}_x(\mathbf{q}) &= \mathbf{J}^{+T}(\mathbf{q})\mathbf{M}(\mathbf{q})\mathbf{J}^+(\mathbf{q}) \\ \mathbf{C}_x(\mathbf{q}, \dot{\mathbf{q}}) &= \mathbf{J}^{+T}(\mathbf{q})(\mathbf{C}(\mathbf{q}, \dot{\mathbf{q}}) - \mathbf{M}(\mathbf{q})\mathbf{J}^+(\mathbf{q})\dot{\mathbf{J}}(\mathbf{q}))\mathbf{J}^+(\mathbf{q}) \\ \mathbf{g}_x(\mathbf{q}) &= \mathbf{J}^{+T}(\mathbf{q})\mathbf{g}(\mathbf{q}) \\ \mathbf{f} &= \mathbf{J}^{+T}(\mathbf{q})\boldsymbol{\tau} \\ \mathbf{f}_e &= \mathbf{J}^{+T}(\mathbf{q})\boldsymbol{\tau}_e \end{aligned} \quad (4)$$

*Remark 1:* In this paper, all the control tasks are designed and achieved in the task space. It will be more convenient to design the controller for pHRI in the task space directly. Therefore, it is necessary to transform the dynamics of a manipulator in the joint space into the dynamics in the task space.

### C. Radial Basis Function Neural Network

RBFNN is commonly utilized to estimate uncertainties in model dynamics, which contains three layers, i.e., the input layer, the hidden layer and the output layer. RBFNN belongs to linear parameterized neural networks, which can be shown as follows [61]:

$$H_i(\mathbf{Z}) = \mathbf{W}_i^T \mathbf{S}_i(\mathbf{Z}), i = 1, 2, \dots, v \quad (5)$$

where  $\mathbf{Z} = [z_1, z_2, \dots, z_p] \in \mathbb{R}^p$  denotes the input vectors and  $p$  is the dimension of  $\mathbf{Z}$ ,  $v$  is the total number of RBFNN,  $\mathbf{W}_i = [w_{i1}, w_{i2}, \dots, w_{il}]^T \in \mathbb{R}^l$  denotes weight vectors in neural networks and  $l$  is the number of RBFNN nodes,  $\mathbf{S}_i(\mathbf{Z}) = [s_1(\mathbf{Z}), s_2(\mathbf{Z}), \dots, s_l(\mathbf{Z})]^T \in \mathbb{R}^l$  denotes the basis functions, and  $s_j(\mathbf{Z}), j = 1, 2, \dots, l$  denotes neuron activation functions. RBFNN is a particular network which uses Gaussian radial basis functions as the basis functions:

$$s_j(\mathbf{Z}) = \exp\left[-\frac{(\mathbf{Z} - \mathbf{o}_j)^T(\mathbf{Z} - \mathbf{o}_j)}{\zeta_j^2}\right], j = 1, 2, \dots, l \quad (6)$$

where  $\mathbf{o}_j = [o_{j1}, o_{j2}, \dots, o_{jp}]^T$  is the centers of the receptive field and  $\varsigma_j$  is Gaussian function's widths. There exist optimal weights  $\mathbf{W}_i^*$  which yields:

$$H_i(\mathbf{Z}) = \mathbf{W}_i^{*T} \mathbf{S}_i(\mathbf{Z}) + \epsilon_i \quad (7)$$

where  $\epsilon_i$  is the approximation errors. The ideal weight vectors  $\mathbf{W}_i^*$  is an artificial quantities for analytical purposes, which is defined as the value of  $\mathbf{W}_i$  that minimizes  $|\epsilon_i|$ :

$$\mathbf{W}_i^* = \arg \min_{\mathbf{W}_i \in \mathbb{R}^l} \{ \sup_{\mathbf{Z} \in \Omega_Z} |\epsilon_i| \} \quad (8)$$

### D. Useful Properties, Assumptions and Lemmas

*Property 1:* The inertia matrices  $\mathbf{M}(\mathbf{q})$  and  $\mathbf{M}_x(\mathbf{q})$  are symmetric positive definite [56].

*Property 2:* The matrix  $\dot{\mathbf{M}}_x(\mathbf{q}) - 2\mathbf{C}_x(\mathbf{q}, \dot{\mathbf{q}})$  is skew symmetric [56].

*Assumption 1:* For the desired trajectory vectors  $\mathbf{x}_d = [x_{d1}, x_{d2}, \dots, x_{dn}]^T$  and constraints  $k_{c_i}$ ,  $i = 1, 2, \dots, n$ , there exist positive constants  $k_{d_i}$ ,  $i = 1, 2, \dots, n$ , such that  $|x_{d_i}| \leq k_{d_i} < k_{c_i}$ ,  $\forall t \geq 0$ .

*Assumption 2:* There exists a positive constant  $\bar{f}_e$  such that  $\|\mathbf{f}_e\| \leq \bar{f}_e$ ,  $\forall t \geq 0$  [56].

*Lemma 1:* [62] For any constants  $k_{c_i}$ ,  $i = 1, 2, \dots, n$ . Let  $\chi := \{\mathbf{x} \in \mathbb{R}^n : |x_i(t)| < k_{c_i}, i = 1, 2, \dots, n, t \geq 0\} \subset \mathbb{R}^n$  and  $\aleph := \mathbb{R}^l \times \chi \subset \mathbb{R}^{l+n}$  be open sets. Then, consider the system as follows:

$$\dot{\eta} = h(t, \eta) \quad (9)$$

where  $\eta := [\omega, \mathbf{x}]^T \in \aleph$ , and  $h : \mathbb{R}_+ \times \aleph \rightarrow \mathbb{R}^{l+n}$  is piecewise continuous in  $t$  and locally Lipschitz in  $\eta$  uniformly in  $t$ , on  $\mathbb{R}_+ \times \aleph$ . Let  $\chi_i := \{x_i \in \mathbb{R} : |x_i(t)| < k_{c_i}, i = 1, 2, \dots, n, t \geq 0\} \subset \mathbb{R}$ . Suppose that there exist functions  $U : \mathbb{R}^l \rightarrow \mathbb{R}_+$  and  $V_i : \chi_i \rightarrow \mathbb{R}_+, i = 1, 2, \dots, n$  continuously differentiable and positive definite in their respective domains, such that

$$V_i \rightarrow \infty \text{ as } |x_i| \rightarrow k_{c_i} \quad (10)$$

$$\gamma_1(\|\omega\|) \leq U(\omega) \leq \gamma_2(\|\omega\|) \quad (11)$$

where  $\gamma_1$  and  $\gamma_2$  are class  $K_\infty$  functions. Let  $V(\eta) := \sum_{i=1}^n V_i(x_i) + U(\omega)$ , and  $x_i(0) \in \chi$ . If the inequality holds:

$$\dot{V} = \frac{\partial V}{\partial \eta} \leq -\mu V + C \quad (12)$$

in the set  $\mathbf{x} \in \chi$ , where  $\mu$  and  $C$  are positive constants, then  $\mathbf{x}(t) \in \chi \forall t \in [0, \infty)$ .

*Lemma 2:* For ensuring the output of system remaining in the constrained task space, we introduce IBLF candidate as

$$V = \sum_{i=1}^n V_i = \sum_{i=1}^n \int_0^{z_i} \frac{\rho k_{c_i}^2}{k_{c_i}^2 - (\rho + \varpi_i)^2} d\rho \quad (13)$$

where  $z_i = x_i - \varpi_i$ , and  $\varpi_i$  is a continuously differentiable function satisfying  $|\varpi_i| < k_{c_i}, i = 1, 2, \dots, n$ . It is known that  $V$  is a continuously positive differentiable functions over the set  $\{|x_i| < k_{c_i}\}$ . As for  $|x_i| < k_{c_i}, i = 1, 2, \dots, n$ , there

is

$$\frac{z_i^2}{2} \leq V_i \leq \frac{k_{c_i}^2 z_i^2}{k_{c_i}^2 - x_i^2} \quad (14)$$

*Proof:* Define

$$p_i(\rho, \varpi_i) = \frac{(\rho k_{c_i}^2)}{k_{c_i}^2 - (\rho + \varpi_i)^2} \quad (15)$$

we can get that

$$\frac{\partial p_i(\rho, \varpi_i)}{\partial \rho} = \frac{k_{c_i}^2 - \rho^2 - \varpi_i^2}{k_{c_i}^2 - (\rho + \varpi_i)^2} \quad (16)$$

which is positive in the set  $|\rho + \varpi_i| < k_{c_i}$ . Since  $p_i(0, \varpi_i)$  for  $|\varpi_i| < k_{c_i}$  and  $p_i(\rho, \varpi_i)$  is increasing with  $\rho$  in the set  $|\rho + \varpi_i| < k_{c_i}$ , we can easily get that

$$\int_0^{z_i} p_i(\rho, \varpi_i) d\rho \leq z_i p_i(z_i, \varpi_i) \quad (17)$$

for  $|z_i + \varpi_i| < k_{c_i}$ . Therefore we can get

$$\int_0^{z_i} \frac{\rho k_{c_i}^2}{k_{c_i}^2 - (\rho + \varpi_i)^2} d\rho \leq \frac{k_{c_i}^2 z_i^2}{k_{c_i}^2 - x_i^2} \quad (18)$$

Then we define

$$\begin{aligned} g(z_i) &= \int_0^{z_i} \frac{\rho k_{c_i}^2}{k_{c_i}^2 - (\rho + \varpi_i)^2} d\rho - \frac{z_i^2}{2} \\ &= \int_0^{z_i} \frac{\rho(\rho + \varpi_i)^2}{k_{c_i}^2 - (\rho + \varpi_i)^2} d\rho \end{aligned} \quad (19)$$

And

$$\frac{\partial g(z_i)}{\partial z_i} = \frac{z_i x_i^2}{k_{c_i}^2 - x_i^2} \quad (20)$$

over the compact set  $\{|x_i| < k_{c_i}\}$ , where  $k_{c_i}^2 - x_i^2 > 0$ . When  $z_i < 0$ , we have  $\frac{\partial g(z_i)}{\partial z_i} < 0$ . When  $z_i > 0$ , we have  $\frac{\partial g(z_i)}{\partial z_i} > 0$ . Since  $z_i = 0$ ,  $g(z_i) = 0$ . Further, there is  $g(z_i) > 0$  over the compact set  $\{|x_i| < k_{c_i}\}$ . Therefore we can get

$$\int_0^{z_i} \frac{\rho k_{c_i}^2}{k_{c_i}^2 - (\rho + \varpi_i)^2} d\rho > \frac{z_i^2}{2} \quad (21)$$

Combining above analysis, *Lemma 2* can be proved.  $\blacksquare$

## III. CONTROL DESIGN

### A. Constrained Space and Reference Trajectory Shaping

To ensure interaction safety, the end-effector of manipulator system should remain within the constrained task space all the time. We firstly shape the reference trajectory to ensure the reference trajectory within the constrained task space subjectively. In order to obtain the reference trajectory  $\mathbf{x}_r$ , we firstly consider a desired admittance model in the task space as follows:

$$\mathbf{M}_d \ddot{\tilde{\mathbf{x}}} + \mathbf{D}_d \dot{\tilde{\mathbf{x}}} + \mathbf{K}_d \tilde{\mathbf{x}} = \mathbf{f}_e \quad (22)$$

where  $\tilde{\mathbf{x}} = \bar{\mathbf{x}}_r - \mathbf{x}_d$ ,  $\bar{\mathbf{x}}_r$  is an intermediate variable vector, and  $\mathbf{x}_d$  is the desired trajectory vector.  $\mathbf{M}_d, \mathbf{D}_d, \mathbf{K}_d$  are desired inertia, damper and stiffness matrices of the desired admittance model, respectively.  $\bar{\mathbf{x}}_r$  can be obtained when  $\mathbf{K}_d, \mathbf{D}_d, \mathbf{M}_d$  and  $\mathbf{x}_d$  are available and  $\mathbf{f}_e$  can be online measured. For simplicity, we

decompose the admittance model into each dimension in the task space and  $\bar{x}_{r_i}$  can be obtained from the admittance model equation

$$K_{m_i}\ddot{\bar{x}}_i + K_{d_i}\dot{\bar{x}}_i + K_{k_i}\bar{x}_i = f_{e_i} \quad i = 1, 2, 3 \quad (23)$$

where  $K_{m_i}, K_{d_i}, K_{k_i}$  are positive constants to guarantee the desired admittance relationship at the end-effector and  $\bar{x}_i = \bar{x}_{r_i} - x_{d_i}$ . For ensuring the reference trajectory remaining in the constrained region, we obtain  $x_{r_i}$  by a soft saturation function as follows:

$$x_{r_i} = \begin{cases} \bar{x}_{r_i} & \text{if } |\bar{x}_{r_i}| \leq \eta k_{c_i} \\ -\theta_i(1 - e^{(\bar{x}_{r_i} + \eta k_{c_i})/\theta_i}) - \eta k_{c_i} & \text{if } \bar{x}_{r_i} < -\eta k_{c_i} \\ \theta_i(1 - e^{(\eta k_{c_i} - \bar{x}_{r_i})/\theta_i}) + \eta k_{c_i} & \text{if } \bar{x}_{r_i} > \eta k_{c_i} \end{cases} \quad (24)$$

where  $i = 1, 2, 3$  and  $\theta_i = (1 - \eta)k_{c_i}$ ,  $\eta$  ( $0 \ll \eta < 1$ ) is a constant very close to 1 and selected to satisfy:

$$|x_{d_i}(t)| \leq k_{d_i} < \eta k_{c_i} \quad \forall t \geq 0 \quad (25)$$

where  $k_{d_i}$  and  $k_{c_i}$  are defined in *Assumption 1*. It is obvious that the soft saturation function ensures  $x_{r_i}$  be twice differentiable and constrained in the task space. The soft saturation function ensures the subjective mobile intention of robotic manipulator  $x_{r_i}$  never goes beyond the constrained boundary and the constraint is preliminarily implemented in path planning. If  $x_i$  tracks  $x_{r_i}$  precisely, the constraints are never violated and admittance relationship can be achieved in the constrained task space.

### B. Control Design with Output Constraint

Because human motion intention is uncertain within the constrained space during pHRI, only reference trajectory shaping cannot ensure the end-effector of robotic manipulators within the constrained space. Besides, unsatisfactory tracking performance under controller will cause large overshoot, which results in that the output of manipulator system is over constraints. Therefore based on the reference trajectory shaping via constructing soft saturation function, other effective methods on constraining system output should be employed in controller design. In our work, IBLF is developed to ensure the output remaining in the predefined task space. To facilitate analysis and explanation, we define  $\mathbf{x}_1 = \mathbf{x}, \mathbf{x}_2 = \dot{\mathbf{x}}$ . The dynamics of manipulator system (3) can be rewritten in state-space form as follows:

$$\begin{aligned} \dot{\mathbf{x}}_1 &= \mathbf{x}_2 \\ \dot{\mathbf{x}}_2 &= \mathbf{M}_x(\mathbf{q})^{-1}(\mathbf{f} - \mathbf{f}_e - \mathbf{g}_x(\mathbf{q}) - \mathbf{C}_x(\mathbf{q}, \dot{\mathbf{q}})\mathbf{x}_2) \end{aligned} \quad (26)$$

We define error variables  $\mathbf{z}_1$  and  $\mathbf{z}_2$  as follows:

$$\begin{aligned} \mathbf{z}_1 &= \mathbf{x}_1 - \mathbf{x}_r \\ \mathbf{z}_2 &= \mathbf{x}_2 - \boldsymbol{\alpha} \end{aligned} \quad (27)$$

where  $\mathbf{z}_1 = [z_{1_1}, z_{1_2}, \dots, z_{1_n}]^T$ ,  $\mathbf{z}_2 = [z_{2_1}, z_{2_2}, \dots, z_{2_n}]^T$ , and  $\boldsymbol{\alpha} = [\alpha_1, \alpha_2, \dots, \alpha_n]^T$  denotes virtual control variable vectors.

One of control objectives is to maintain system output  $\mathbf{x}_1$  be constrained in the constrained region, namely  $|x_{1_i}| <$

$k_{c_i}, i = 1, 2, 3$ . To avoid violating constraints, we consider IBLF candidate as follows:

$$V_1 = \sum_{i=1}^n \int_0^{z_{1_i}} \frac{\rho k_{c_i}^2}{k_{c_i}^2 - (\rho + x_{r_i})^2} d\rho \quad (28)$$

The time derivative of  $V_1$  yields

$$\dot{V}_1 = \sum_{i=1}^n \frac{z_{1_i} k_{c_i}^2}{k_{c_i}^2 - x_{1_i}^2} \dot{z}_{1_i} + \sum_{i=1}^n \frac{\partial V_1}{\partial x_{r_i}} \dot{x}_{r_i} \quad (29)$$

where

$$\frac{\partial V_1}{\partial x_{r_i}} = z_{1_i} \left( \frac{k_{c_i}^2}{k_{c_i}^2 - x_{1_i}^2} - \lambda_i \right) \quad (30)$$

$$\lambda_i = \frac{k_{c_i}}{2z_{1_i}} \ln \frac{(k_{c_i} + z_{1_i} + x_{r_i})(k_{c_i} - x_{r_i})}{(k_{c_i} - z_{1_i} - x_{r_i})(k_{c_i} + x_{r_i})} \quad (31)$$

*Remark 2:* In (31),

$$\lim_{z_{1_i} \rightarrow 0} \frac{k_{c_i}}{2z_{1_i}} \ln \frac{(k_{c_i} + z_{1_i} + x_{r_i})(k_{c_i} - x_{r_i})}{(k_{c_i} - z_{1_i} - x_{r_i})(k_{c_i} + x_{r_i})} = \frac{k_{c_i}^2}{k_{c_i}^2 - x_{r_i}^2}$$

. Therefore, the singularity for this term will not happen.

We design the virtual control variable  $\alpha_i$  as follows:

$$\alpha_i = -k_i z_{1_i} + \frac{(k_{c_i}^2 - x_{1_i}^2) \dot{x}_{r_i} \lambda_i}{k_{c_i}^2} \quad (32)$$

where  $k_i, i = 1, 2, \dots, n$  are positive constants. Substituting (32) into (29), we can get

$$\dot{V}_1 = - \sum_{i=1}^n \frac{k_i z_{1_i}^2 k_{c_i}^2}{k_{c_i}^2 - x_{1_i}^2} + \sum_{i=1}^n \frac{z_{1_i} z_{2_i} k_{c_i}^2}{k_{c_i}^2 - x_{1_i}^2} \quad (33)$$

Then we design  $V_2$  as follows:

$$V_2 = V_1 + \frac{1}{2} \mathbf{z}_2^T \mathbf{M}_x(\mathbf{q}) \mathbf{z}_2 \quad (34)$$

the derivative with time of  $V_2$  is

$$\begin{aligned} \dot{V}_2 &= \dot{V}_1 + \mathbf{z}_2^T \mathbf{M}_x(\mathbf{q}) \dot{\mathbf{z}}_2 + \frac{1}{2} \mathbf{z}_2^T \dot{\mathbf{M}}_x(\mathbf{q}) \mathbf{z}_2 \\ &= - \sum_{i=1}^n \frac{k_i z_{1_i}^2 k_{c_i}^2}{k_{c_i}^2 - x_{1_i}^2} + \sum_{i=1}^n \frac{z_{1_i} z_{2_i} k_{c_i}^2}{k_{c_i}^2 - x_{1_i}^2} \\ &\quad + \mathbf{z}_2^T (\mathbf{f} - \mathbf{f}_e - \mathbf{g}_x(\mathbf{q}) - \mathbf{C}_x(\mathbf{q}, \dot{\mathbf{q}})\mathbf{x}_2 \\ &\quad - \mathbf{M}_x(\mathbf{q})\dot{\boldsymbol{\alpha}}) + \frac{1}{2} \mathbf{z}_2^T \dot{\mathbf{M}}_x(\mathbf{q}) \mathbf{z}_2 \end{aligned} \quad (35)$$

and design the control input  $\mathbf{f} = \mathbf{f}_m$  as follows:

$$\mathbf{f}_m = - \begin{pmatrix} \frac{z_{1_1} k_{c_1}^2}{k_{c_1}^2 - x_{1_1}^2} \\ \frac{z_{1_2} k_{c_2}^2}{k_{c_2}^2 - x_{1_2}^2} \\ \vdots \\ \frac{z_{1_n} k_{c_n}^2}{k_{c_n}^2 - x_{1_n}^2} \end{pmatrix} - \mathbf{K}_2 \mathbf{z}_2 + \mathbf{f}_e + \mathbf{g}_x(\mathbf{q}) + \mathbf{C}_x(\mathbf{q}, \dot{\mathbf{q}})\boldsymbol{\alpha} + \mathbf{M}_x(\mathbf{q})\dot{\boldsymbol{\alpha}} \quad (36)$$

where the positive gain matrix  $\mathbf{K}_2 > 0$ . The model-based controller can ensure that  $\mathbf{z}_1$  and  $\mathbf{z}_2$  will converge to zero and  $\mathbf{x}_1$  can remain in the predefined constrained space. The proof of stability is shown in Appendix I. From the engineering point of view, model-based control input (36) cannot be designed in

practical applications [56]. To address the uncertainty issue in the dynamic model, RBFNN is utilized to approximate uncertainties of manipulators. RBFNN can improve the tracking precision when the manipulator system tracks  $x_r$ . An adaptive NN control input is proposed as follows:

$$f = - \begin{pmatrix} \frac{z_{11} k_{c1}^2}{k_{c1}^2 - x_{11}^2} \\ \frac{z_{12} k_{c2}^2}{k_{c2}^2 - x_{12}^2} \\ \vdots \\ \frac{z_{1n} k_{cn}^2}{k_{cn}^2 - x_{1n}^2} \end{pmatrix} - K_2 z_2 + f_e + \hat{W}^T S(Z) \quad (37)$$

where  $\hat{W}$  is the estimated weight of RBFNN,  $S(Z)$  denotes the basis function and  $Z = [q^T, \dot{q}^T, \alpha^T, \dot{\alpha}^T]^T$  is the input variable. The adaptive updating laws are designed as follows:

$$\dot{\hat{W}}_i = -\Gamma_i (S_i(Z) z_{2i} + \varphi_i \hat{W}_i) \quad (38)$$

where  $\Gamma_i, i = 1, 2, \dots, n$  are positive definite symmetric matrices and  $\varphi_i$  are small positive constants.  $\hat{W}^T S(Z)$  is used to estimate  $W^{*T} S(Z)$  which is defined as follows:

$$W^{*T} S(Z) = g_x(q) + C_x(q, \dot{q})\alpha + M_x(q)\dot{\alpha} - \epsilon \quad (39)$$

where  $\epsilon$  is approximation error and  $W^*$  is the optimal weight of RBFNN. The  $\tilde{W} = \hat{W} - W^*$  denotes the error of weight. The adaptive NN controller with the adaptation law can ensure that  $z_{1i}$ ,  $z_2$  and  $\tilde{W}_i$  are SGUUB [56] and  $x_{1i}$  can remain in the constrained task space. The analysis of stability is carried out by a new BLF candidate  $V_3 = V_2 + \frac{1}{2} \sum_{i=1}^n \tilde{W}_i^T \Gamma_i^{-1} \tilde{W}_i$ . The proof of stability is shown in Appendix II.

*Theorem 1:* For the manipulator system, given the initial conditions are bounded, the proposed controller (37) with adaptive law (38) ensures that  $z_{1i}$ ,  $z_2$  and  $\tilde{W}_i$  are SGUUB [56] and  $x_{1i}$  can remain in the constrained task space. The closed-loop error signals will remain within the compact sets  $\Omega_{z_1}$ ,  $\Omega_{z_2}$  and  $\Omega_{\tilde{W}}$ , respectively and defined by

$$\Omega_{z_1} = \left\{ z_1 \in \mathbb{R}^n \mid |z_{1i}| \leq \sqrt{H}, i = 1, 2, \dots, n \right\} \quad (40)$$

$$\Omega_{z_2} = \left\{ z_2 \in \mathbb{R}^n \mid \|z_2\| \leq \sqrt{\frac{H}{\lambda_{\min}(M_x(q))}} \right\} \quad (41)$$

$$\Omega_{\tilde{W}} = \left\{ \tilde{W} \in \mathbb{R}^{l \times n} \mid \|\tilde{W}\| \leq \sqrt{\frac{H}{\lambda_{\min}(\Gamma^{-1})}} \right\} \quad (42)$$

where  $H = 2(V_3(0) + C_3/\mu_3)$ .  $C_3$  and  $\mu_3$  are given in (51). The proof of convergence is shown in Appendix III.

*Remark 3:* The proposed control architecture is shown in Fig. 2. Under our proposed controller, the control objective is achieved that the manipulator can track the shaped virtual trajectory precisely in the task space via neural network learning approach, and all error signals are SGUUB, which means that the desired admittance relationship of a manipulator can be achieved. On the other hand, the controller simultaneously guarantees that the end-effector of manipulator system remains in the constrained task space strictly by virtual trajectory shaping and IBLF method.

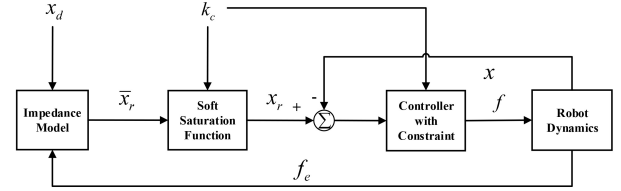


Fig. 2: Control architecture.

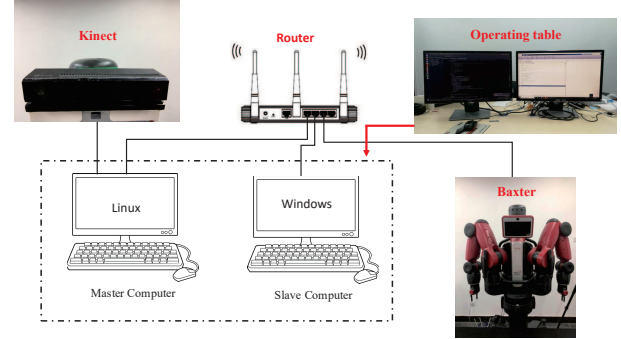


Fig. 3: Experimental platform: it is composed of Baxter robot, Kinect camera, a master computer, a slave computer, etc.

## IV. EXPERIMENTS

In this paper, Baxter robot is employed to verify our proposed control algorithm. The robotic manipulator has 7 flexible joints with advanced sensors, including position, velocity, torque sensors. Joint sensor resolution is 14 bits with 360 degrees (0.022 degrees per tick resolution). Every joint can be driven by a torque controller. The designed experimental platform shown as Fig. 3 is composed of a Baxter robot, a Kinect camera, a master computer, a slave computer, etc.

Two computers are used in the experimental system. The master computer is employed to receive datas from Baxter robot, run main programs and send control command to robot. The slave computer receives datas from the master computer, calculates NN compensation and transfers calculation results to master computer by user datagram protocol (UDP).

Experiment is desired to verify that the manipulator can interact with human operator when the manipulator is operated within the constrained space obediently. In addition, the end-effector of manipulator can remain in the constrained space to ensure safety. In this experiment, we only use the right arm of the Baxter robot and operate the robotic manipulator in the task space.

### A. The Design and Setting of Experiment

In control design part, we design an adaptive NN admittance controller with output constraint and have analysed the stability of the system with the proposed controller by Lyapunov method. We transform force control input  $f$  into torque input  $\tau$  in the joint torque controller as  $\tau = J^T(q)f$  according to (4),  $J^T(q)$  can be obtained from ROS packages. In this part, we apply the designed torque controller on Baxter robot to verify the proposed algorithm in experiment. Initially, the end-effector stays in the initial position

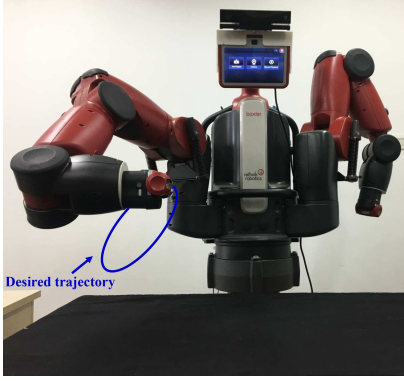


Fig. 4: Schematic diagram of tracking test.

$\mathbf{x}(0) = [-0.13(\text{m}), -0.4(\text{m}), 0.74(\text{m})]$ . Control parameters are chosen as  $k_1 = 17.7, k_2 = 15, k_3 = 22$  and  $\mathbf{K}_2 = \text{diag}[5.1, 12, 4.5]$ . After our repeated verification, the number of RBFNN nodes is chosen as  $\text{Node} = 729$ . In this number settings, we can obtain great estimated results and the computing time is within acceptable range. The centers of RBFNN nodes are evenly designed between the upper and lower bounds of the motion range and speed limits separately in joint space and task space, in  $[-1.7, 1.7] \times [-2.1, 1.0] \times [-3.1, 3.1] \times [0.0, 2.6] \times [-3.1, 3.1] \times [-1.6, 2.1] \times [-3.1, 3.1] \times [-0.5, 0.5] \times [-1, 0] \times [0.5, 1.5]$  and  $[-2.0, 2.0] \times [-2.0, 2.0] \times [-2.0, 2.0] \times [-2.0, 2.0] \times [-4.0, 4.0] \times [-4.0, 4.0] \times [-4.0, 4.0] \times [-0.5, 0.5] \times [-0.5, 0.5] \times [-0.5, 0.5]$ . The settings of centers can ensure the RBFNN traversing the whole joint space, task space and operating speed space which generates good estimated results. All initial values of RBFNN weights are set as 0. Parameters of adaptive law are  $\mathbf{\Gamma}_i = 100\mathbf{I}_{\text{Node}}$  and  $\varphi_i = 0.002$ . The desired trajectory in the task space is described by

$$\begin{aligned} x_{d_x}(t) &= (0.15 \sin(50\pi/t) - 0.1)(\text{m}) \\ x_{d_y}(t) &= (0.2 \cos(50\pi/t) - 0.6)(\text{m}) \\ x_{d_z}(t) &= (0.2 \sin(50\pi/t) + 0.75)(\text{m}) \end{aligned} \quad (43)$$

Then, reference trajectory  $\mathbf{x}_r$  can be obtained by the predefined admittance model and the soft saturation function. Parameters of admittance model are designed as  $k_{m_i} = 1, k_{d_i} = 10$  and  $k_{k_i} = 30, i = 1, 2, 3$ . Parameter of soft saturation function is chosen as  $\eta = 0.97$  and it is obvious that  $k_{d_i} = \max\{|x_{d_i}(t)|\}$ .

*Remark 4:* In experiments, the maximum external forces are 16.5N, 24N and 28.5N separately in X-axis, Y-axis and Z-axis. External forces can not exceed thresholds under normal operation. The disturbance force will not influence the experimental performance by setting stiffness parameters of admittance model as 30 N/m.

### B. Case 1. Tracking test.

In this part, we only consider the end-effector of Baxter robot tracking the reference trajectory without interaction as shown in Fig. 4. The tracking performances in X-axis, Y-axis and Z-axis are shown in Fig. 5(a), Fig. 5(c) and Fig. 5(e), where the green, red and black lines represent the actual,

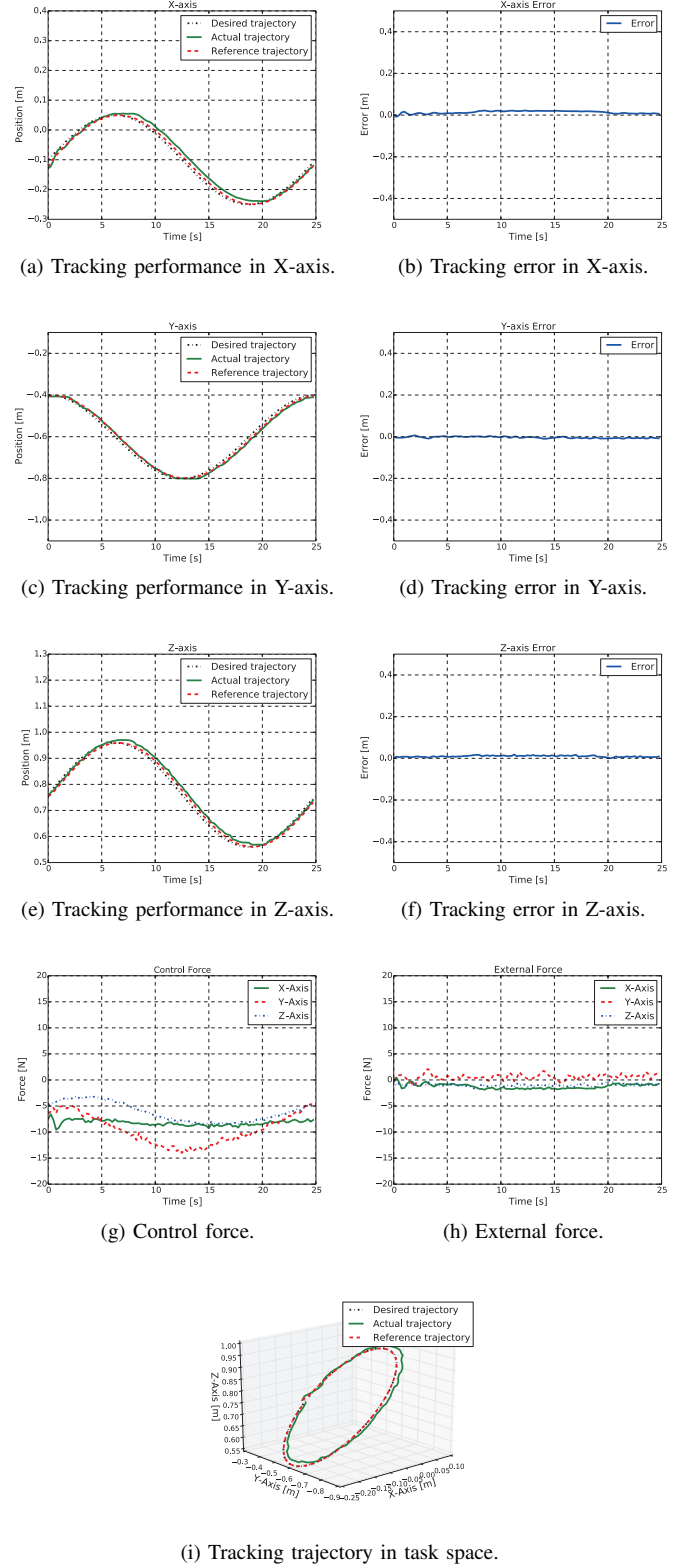


Fig. 5: The results of tracking test.

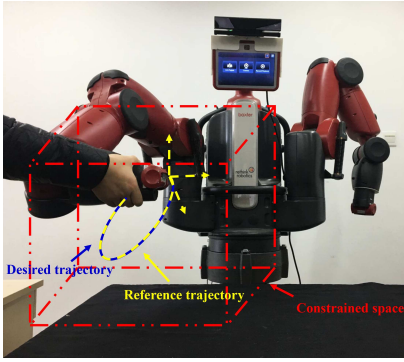
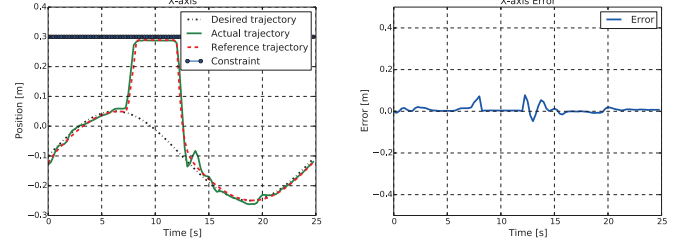


Fig. 6: Schematic diagram of human-robot interaction within the constrained space.

reference and desired trajectories, respectively. The tracking error results are shown in Fig. 5(b), Fig. 5(d) and Fig. 5(f) correspondingly. The position tracking performance in the task space is shown as Fig. 5(i). It is obvious that the manipulator under the our proposed controller shows a good tracking performance in real time. The reference trajectory  $x_r$  in every axis is the same as the desired trajectory  $x_d$  without interaction. Control force are shown in Fig. 5(g). External forces caused by small disturbances are near zero which can be ignored shown as Fig. 5(h). It shows that neural learning approach can solve uncertainties in dynamics of manipulator system, whose results are in a good tracking performance.

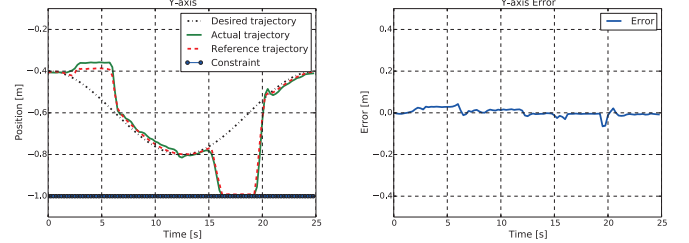
### C. Case 2. Human-robot interaction test within the constrained space.

In this part, the robotic manipulator interacts with a human operator to perform tasks collaboratively. The control objective is to make the robotic manipulator comply with human operator and within the predefined constrained space as shown in Fig. 6. Constraints are set as  $k_{c1} = 0.3(\text{m})$ ,  $k_{c2} = 1(\text{m})$  and  $k_{c3} = 1.2(\text{m})$  in each dimension, respectively. The human operates the manipulator towards constrained boundaries in X-axis, Y-axis and Z-axis orderly. The tracking performances in X-axis, Y-axis and Z-axis are shown in Fig. 7(a), Fig. 7(c) and Fig. 7(e) where the green, red, black and blue lines represent the actual, reference, desired trajectories and constraint, respectively. The tracking errors in three axes converge to zero indicated from Fig. 7(b), Fig. 7(d) and Fig. 7(f), correspondingly. The position tracking performance in the task space is shown in Fig. 7(i). It is obvious that the reference trajectory  $x_r$  varies with the external force. According to the admittance model and the soft saturation function, the reference trajectory is obtained to comply with the mobile intention of human and maintain the end-effector within constrained boundary. Above results demonstrate that our proposed controller ensures the end-effector tracking the reference trajectory in real time within the constrained space. As shown in Fig. 7(g), control forces in three axes are in proper values whether there is interaction or not during the task. As shown in Fig. 7(h), interaction forces in three axes are in proper values which will not bring uncomfortable feelings to human operators. On the basis of results, we can



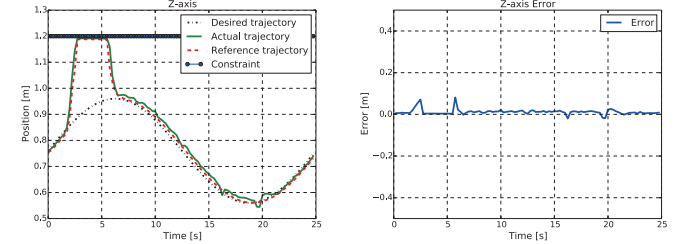
(a) Tracking trajectory and constraint in X-axis.

(b) Tracking error in X-axis.



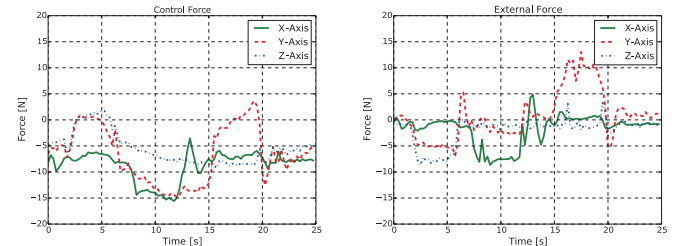
(c) Tracking trajectory and constraint in Y-axis.

(d) Tracking error in Y-axis.



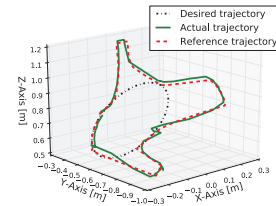
(e) Tracking trajectory and constraint in Z-axis.

(f) Tracking error in Z-axis.



(g) Control force.

(h) External force.



(i) Tracking trajectory in task space.

Fig. 7: The results of human-robot interaction test within the constrained space.

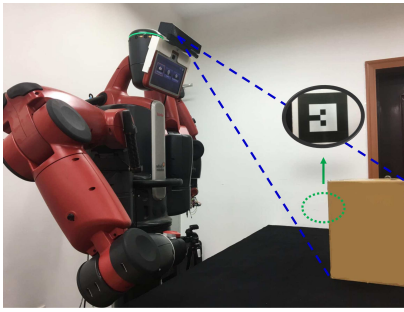


Fig. 8: Obtaining constrained boundary by Kinect camera.

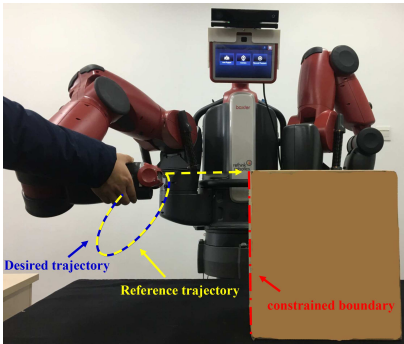


Fig. 9: Schematic diagram of human-robot interaction within constrained space to avoid collision.

give a summary that our proposed controller can ensure the end-effector of Baxter robot not only tracking the reference trajectory in a good performance but also complying with human in the constrained task space.

*D. Case 3. Human-robot interaction test within the constrained space to avoid collisions.*

In this part, Kinect camera and quick response (QR) code are utilized to get the obstacle location and we transfer the obtained data to the master computer. The obstacle location at Kinect coordinate system can be transformed to the coordinate at Baxter coordinate system through a transformation matrix. We place the Kinect on the head of the Baxter robot and paste a QR code on the edge of the obstacle so that the Kinect camera can obtain the position information of the

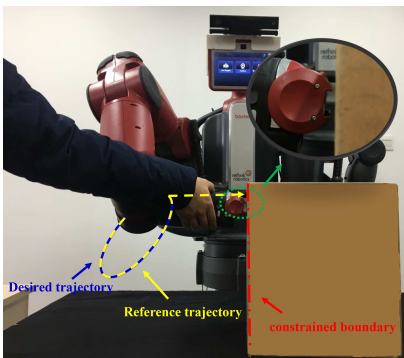
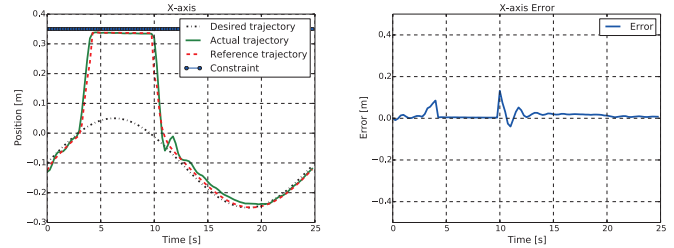
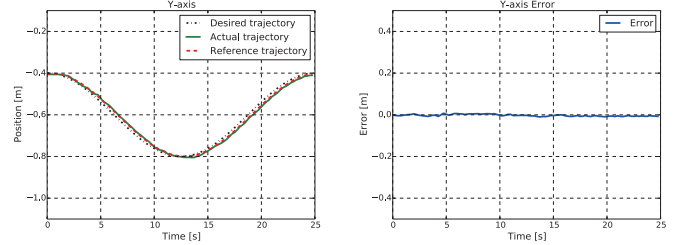


Fig. 10: The experimental results within constrained space to avoid collision.



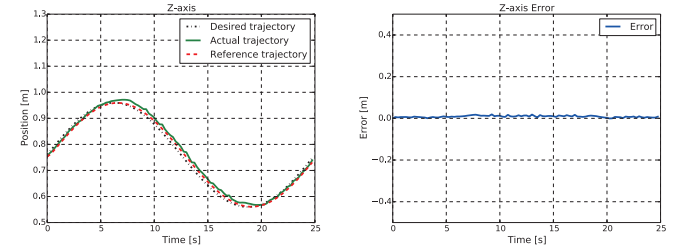
(a) Tracking trajectory and constraint in X-axis.

(b) Tracking error in X-axis.



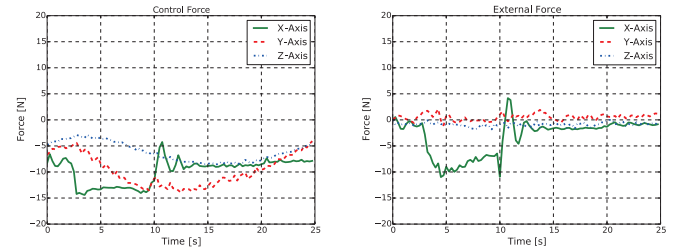
(c) Tracking trajectory and constraint in Y-axis.

(d) Tracking error in Y-axis.



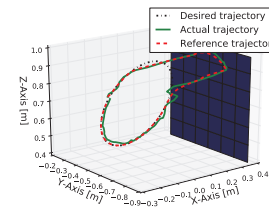
(e) Tracking trajectory and constraint in Z-axis.

(f) Tracking error in Z-axis.



(g) Control force.

(h) External force.



(i) Tracking trajectory in task space.

Fig. 11: The results of human-robot interaction test within the constrained space to avoid collision.

obstacle which is in front of Baxter robot, shown in Fig. 8. For simplicity, we only avoid collisions in X-axis and do not consider the constraint in Y-axis and Z-axis in this experiment. Using our proposed method, we get the constrained boundary in X-axis  $k_{c_1} = 0.35\text{m}$  in advance by the Kinect camera and common filtering algorithm. In other words, our control objective in this experimental part is that the end-effector of Baxter robot cannot beyond the constrained boundary in X-axis to avoid collisions with obstacle. As shown in Fig. 9, human operator interacts with the end-effector of Baxter robot and move it towards the obstacle. The experiment results are shown in Fig. 10. We can see that the end-effector cannot be operated beyond the constrained boundary under our proposed controller. Larger interaction force cannot drive the robot colliding with the obstacle either. The tracking performances of X-axis, Y-axis and Z-axis are shown in Fig. 11(a), Fig. 11(c) and Fig. 11(e) where the green, red, black and blue lines represent the actual, reference, desired trajectories and constrained boundary, respectively. The tracking error results are shown in Fig. 11(b), Fig. 11(d) and Fig. 11(f) correspondingly. It is similar to *Case 2* that the reference trajectory varies with the external force in X-axis. According to the admittance model and the soft saturation function, the reference trajectory is obtained to comply with the mobile intention of human and keep the end-effector within the constrained boundary. It is obvious that the end-effector of Baxter robot is constrained within the constrained boundary to avoid collisions with the obstacle. In this experiment, because of no interaction in Y-axis and Z-axis, the reference trajectories  $\mathbf{x}_r$  on these axes are the same as the desired trajectory  $\mathbf{x}_d$ . The position trajectory performance in the task space is shown in Fig. 11(i), where the blue plane respects the obstacle. As shown in Fig. 11(g), control forces in three axes are in proper values whether there is interaction or not during the task. The interaction force is shown as Fig. 11(h) which will not bring uncomfortable feelings to human operators. On the basis of results, we can give a summary that the proposed method can ensure operated safety during the process of pHRI, and the end-effector of the robotic manipulator can avoid the obstacle successfully in the task space rely on the additional visual sensory information.

### E. Conclusion of Experiments

On the basis of above analysis and compared experimental results, we can conclude that the proposed control algorithm can ensure the end-effector of the manipulator complying with operators and ensure operation safety. It has great performances of tracking and complying when the manipulator is operated within the constrained task space. We can draw the conclusion that the end-effector of Baxter robot does not exceed the constrained space, and collisions can be avoided relying on visual feedback under our proposed controller design. The achieved admittance relationship makes the end-effector of Baxter robot reflect compliance in pHRI.

## V. CONCLUSION

In this paper, a shaping reference trajectory by a soft saturation function has been designed in path planning. An

admittance-based controller involving IBLF has been applied in pHRI and RBFNN learning method has been proposed to approximate dynamics uncertainties. Our proposed controller has guaranteed the end-effector of the manipulator in the constrained task space and improved the compliance of interaction. The effectiveness has been verified on Baxter robot experiment platform in three cases. In our future work, we will further research on the redundancy problem of manipulator and focus on time-varying constrained BLF methods. We will also try to propose an advanced controller for pHRI to avoid collisions in a dynamical scenario where the obstacle position is time-varying.

### ACKNOWLEDGMENTS

The authors would like to sincerely thank the Editor-In-Chief, the Editor, the Associate Editor and the anonymous reviewers for their constructive comments which helped improve the quality and presentation of this paper.

### APPENDIX I

*Proof:* Substituting (32) and (36) into (35), we can get

$$\dot{V}_2 = - \sum_{i=1}^n \frac{k_i z_{1_i}^2 k_{c_i}^2}{k_{c_i}^2 - x_{1_i}^2} - \mathbf{z}_2^T \mathbf{K}_2 \mathbf{z}_2 \quad (44)$$

Considering *Lemma 2*, we can get:

$$\begin{aligned} \dot{V}_2 &\leq - \sum_{i=1}^n \int_0^{z_{1_i}} \frac{\rho k_i k_{c_i}^2}{k_{c_i}^2 - (\rho + x_{r_i})^2} d\rho - \mathbf{z}_2^T \mathbf{K}_2 \mathbf{z}_2 \\ &\leq -\mu_2 V_2 \end{aligned} \quad (45)$$

where  $\mu_2$  is a constant defined as

$$\mu_2 = \min \left( \min_{i=1,2,\dots,n} (k_i), \frac{2\lambda_{\min}(\mathbf{K}_2)}{\lambda_{\max}(\mathbf{M}_x(\mathbf{q}))} \right) \quad (46)$$

To ensure  $\mu_2 > 0$ , control parameters  $k_i$  and positive gain matrix  $\mathbf{K}_2$  should be satisfied

$$\min(k_i) > 0, \lambda_{\min}(\mathbf{K}_2) > 0, i = 1, 2, \dots, n$$

It is obvious that  $V_2$  will converge to zero. Hence  $\mathbf{z}_1$  and  $\mathbf{z}_2$  will converge to zero and  $\mathbf{x}_1$  can remain in the predefined constrained space according to the *Lemma 1*. ■

### APPENDIX II

*Proof:* To prove the stability of close-loop system, we construct a new IBLF candidate  $V_3$  as follows:

$$V_3 = V_2 + \frac{1}{2} \sum_{i=1}^n \tilde{\mathbf{W}}_i^T \Gamma_i^{-1} \tilde{\mathbf{W}}_i \quad (47)$$

where  $\tilde{\mathbf{W}} = \hat{\mathbf{W}} - \mathbf{W}^*$  denotes errors of weights, then differentiating  $V_3$  yields:

$$\begin{aligned} \dot{V}_3 &= - \sum_{i=1}^n \frac{k_i z_{1_i}^2 k_{c_i}^2}{k_{c_i}^2 - x_{1_i}^2} + \sum_{i=1}^n \frac{z_{1_i} z_{2_i} k_{c_i}^2}{k_{c_i}^2 - x_{1_i}^2} + \mathbf{z}_2^T (\mathbf{f} - \mathbf{f}_e) \\ &\quad - \mathbf{g}_x(\mathbf{q}) - \mathbf{C}_x(\mathbf{q}, \dot{\mathbf{q}}) \boldsymbol{\alpha} - \mathbf{M}_x(\mathbf{q}) \dot{\boldsymbol{\alpha}} \\ &\quad + \sum_{i=1}^n \tilde{\mathbf{W}}_i^T \Gamma_i^{-1} \dot{\tilde{\mathbf{W}}}_i \end{aligned} \quad (48)$$

Substituting (37) into  $\dot{V}_3$ , we obtain

$$\begin{aligned} \dot{V}_3 = & - \sum_{i=1}^n \frac{k_i z_{1_i}^2 k_{c_i}^2}{k_{c_i}^2 - x_{1_i}^2} - \mathbf{z}_2^T \mathbf{K}_2 \mathbf{z}_2 + \mathbf{z}_2^T (\hat{\mathbf{W}}^T \mathbf{S}(\mathbf{Z}) \\ & - \mathbf{W}^{*T} \mathbf{S}(\mathbf{Z}) - \boldsymbol{\epsilon}) - \sum_{i=1}^n \tilde{\mathbf{W}}_i^T (\mathbf{S}_i(\mathbf{Z}) z_{2_i} + \varphi_i \hat{\mathbf{W}}_i) \end{aligned} \quad (49)$$

Since inequality relation:

$$\begin{aligned} -\mathbf{z}_2^T \boldsymbol{\epsilon} & \leq \frac{1}{2} \mathbf{z}_2^T \mathbf{z}_2 + \frac{1}{2} \|\bar{\boldsymbol{\epsilon}}\|^2 \\ -\varphi_i \tilde{\mathbf{W}}_i^T \hat{\mathbf{W}}_i & \leq \frac{\varphi_i}{2} (\|\mathbf{W}_i^*\|^2 - \|\tilde{\mathbf{W}}_i\|^2) \end{aligned}$$

where  $\|\boldsymbol{\epsilon}\| \leq \|\bar{\boldsymbol{\epsilon}}\|$ ,  $\bar{\boldsymbol{\epsilon}}$  is the upper limit of error. We further have

$$\begin{aligned} \dot{V}_3 & \leq - \sum_{i=1}^n \int_0^{z_{1_i}} \frac{\rho k_i k_{c_i}^2}{k_{c_i}^2 - (\rho + x_{1_i})^2} d\rho - \mathbf{z}_2^T (\mathbf{K}_2 - \frac{1}{2} \mathbf{I}) \mathbf{z}_2 \\ & - \sum_{i=1}^n \frac{\varphi_i}{2} \|\tilde{\mathbf{W}}_i\|^2 + \sum_{i=1}^n \frac{\varphi_i}{2} \|\mathbf{W}_i^*\|^2 + \frac{1}{2} \|\bar{\boldsymbol{\epsilon}}\|^2 \\ & \leq -\mu_3 V_3 + C_3 \end{aligned} \quad (50)$$

where

$$\begin{aligned} \mu_3 & = \min \left( \min_{i=1,2,\dots,n} (k_i), \frac{2(\lambda_{\min}(\mathbf{K}_2 - \frac{1}{2} \mathbf{I}))}{\lambda_{\max}(\mathbf{M}_x(\mathbf{q}))}, \right. \\ & \left. \min_{i=1,2,\dots,n} \left( \frac{\varphi_i}{\lambda_{\max}(\boldsymbol{\Gamma}_i^{-1})} \right) \right) \\ C_3 & = \sum_{i=1}^n \frac{\varphi_i}{2} \|\mathbf{W}_i^*\|^2 + \frac{1}{2} \|\bar{\boldsymbol{\epsilon}}\|^2 \end{aligned} \quad (51)$$

To ensure  $\mu_3 > 0$ , gain parameters  $k_i$ , positive gain matrix  $\mathbf{K}_2$  and  $\varphi_i$  should be chosen to satisfy:

$$\min(k_i) > 0, \lambda_{\min}(\mathbf{K}_2 - \frac{1}{2} \mathbf{I}) > 0, \min(\varphi_i) > 0, i = 1, 2, \dots, n$$

### APPENDIX III

*Proof:* Multiplying (50) by  $e^{\mu_3 t}$  yields

$$\dot{V}_3 e^{\mu_3 t} \leq -\mu_3 V_3 e^{\mu_3 t} + C_3 e^{\mu_3 t} \quad (52)$$

$$\frac{d}{dt} (V_3 e^{\mu_3 t}) \leq C_3 e^{\mu_3 t} \quad (53)$$

Integrating the above inequality, we obtain

$$V_3 e^{\mu_3 t} - V_3(0) \leq \frac{C_3}{\mu_3} e^{\mu_3 t} - \frac{C_3}{\mu_3} \quad (54)$$

$$V_3 \leq (V_3(0) - \frac{C_3}{\mu_3}) e^{-\mu_3 t} + \frac{C_3}{\mu_3} \leq V(0) + \frac{C_3}{\mu_3} \quad (55)$$

Therefore, we have

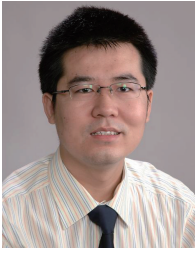
$$\frac{1}{2} |z_{1_i}|^2 \leq V_3(0) + \frac{C_3}{\mu_3} \quad (56)$$

Hence,  $z_{1_i}$  converges to the compact set  $\Omega_{z_1}$ . Bounds for  $\mathbf{z}_2$  and  $\tilde{\mathbf{W}}_i$  can be proven similarly. ■

### REFERENCES

- [1] A. U. Pehlivan, D. P. Losey, and M. K. O'Malley, "Minimal assist-as-needed controller for upper limb robotic rehabilitation," *IEEE Transactions on Robotics*, vol. 32, no. 1, pp. 113–124, 2016.
- [2] H. Yu, S. Huang, G. Chen, Y. Pan, and Z. Guo, "Human-robot interaction control of rehabilitation robots with series elastic actuators," *IEEE Transactions on Robotics*, vol. 31, no. 5, pp. 1089–1100, 2015.
- [3] W. He, W. Ge, Y. Li, Y.-J. Liu, C. Yang, and C. Sun, "Model identification and control design for a humanoid robot," *IEEE Transactions on Systems, Man, and Cybernetics: Systems*, vol. 47, no. 1, pp. 45–57, 2017.
- [4] Z. Li, H. Bo, A. Ajoudani, C. Yang, C. Y. Su, and A. Bicchi, "Asymmetric bimanual control of dual-arm exoskeletons for human-cooperative manipulations," *IEEE Transactions on Robotics*, vol. 34, no. 1, pp. 264–271, 2018.
- [5] T. Zhang, X. Wang, X. Xu, and C. P. Chen, "GCB-Net: Graph convolutional broad network and its application in emotion recognition," *IEEE Transactions on Affective Computing*, 2019, DOI: 10.1109/TAFFC.2019.2937768.
- [6] T. Zhang, G. Su, C. Qing, X. Xu, B. Cai, and X. Xing, "Hierarchical lifelong learning by sharing representations and integrating hypothesis," *IEEE Transactions on Systems, Man, and Cybernetics: Systems*, 2019, DOI: 10.1109/TSMC.2018.2884996.
- [7] C. Yang, H. Wu, Z. Li, H. Wei, W. Ning, and C. Y. Su, "Mind control of a robotic arm with visual fusion technology," *IEEE Transactions on Industrial Informatics*, vol. 14, no. 9, pp. 3822–3830, 2017.
- [8] Z. Li, T. Zhao, F. Chen, Y. Hu, C. Y. Su, and T. Fukuda, "Reinforcement learning of manipulation and grasping using dynamical movement primitives for a humanoid-like mobile manipulator," *IEEE/ASME Transactions on Mechatronics*, vol. 23, no. 1, pp. 121–131, 2018.
- [9] Q. Shi, C. Li, K. Li, Q. Huang, H. Ishii, A. Takamishi, and T. Fukuda, "A modified robotic rat to study rat-like pitch and yaw movements," *IEEE/ASME Transactions on Mechatronics*, vol. 23, no. 5, pp. 2448–2458, 2018.
- [10] Z. Chao, Y. Chenguang, and C. Zhaopeng, "Bio-inspired robotic impedance adaptation for human-robot collaborative tasks," *SCIENCE CHINA Information Sciences*, 2020, DOI: 10.1007/s11432-019-2748-x.
- [11] M. H. Raibert and J. J. Craig, "Hybrid position/force control of manipulators," *Journal of Dynamic Systems, Measurement, and Control*, vol. 103, no. 2, pp. 126–133, 1981.
- [12] M. C. Yip and D. B. Camarillo, "Model-less hybrid position/force control: A minimalist approach for continuum manipulators in unknown, constrained environments," *IEEE Robotics and Automation Letters*, vol. 1, no. 2, pp. 844–851, 2016.
- [13] C. Yang, C. Zeng, P. Liang, Z. Li, R. Li, and C.-Y. Su, "Interface design of a physical human-robot interaction system for human impedance adaptive skill transfer," *IEEE Transactions on Automation Science and Engineering*, vol. 15, no. 1, pp. 329–340, 2018.
- [14] D. Heck, A. Saccon, N. Van de Wouw, and H. Nijmeijer, "Guaranteeing stable tracking of hybrid position-force trajectories for a robot manipulator interacting with a stiff environment," *Automatica*, vol. 63, pp. 235–247, 2016.
- [15] N. Hogan, "Impedance control: An approach to manipulation: Part II-implementation," *Journal of Dynamic Systems, Measurement, and Control*, vol. 107, no. 1, pp. 8–16, 1985.
- [16] K. Hashtrudi-Zaad and S. E. Salcudean, "Analysis of control architectures for teleoperation systems with impedance/admittance master and slave manipulators," *The International Journal of Robotics Research*, vol. 20, no. 6, pp. 419–445, 2001.
- [17] M. A. Goodrich, A. C. Schultz, *et al.*, "Human-robot interaction: a survey," *Foundations and Trends in Human-Computer Interaction*, vol. 1, no. 3, pp. 203–275, 2008.
- [18] F. Ficuciello, L. Villani, and B. Siciliano, "Variable impedance control of redundant manipulators for intuitive human-robot physical interaction," *IEEE Transactions on Robotics*, vol. 31, no. 4, pp. 850–863, 2015.
- [19] F. Ficuciello, A. Romano, L. Villani, and B. Siciliano, "Cartesian impedance control of redundant manipulators for human-robot co-manipulation," in *Intelligent Robots and Systems (IROS 2014), 2014 IEEE/RSJ International Conference on*, pp. 2120–2125, IEEE, 2014.
- [20] I. Ranatunga, F. L. Lewis, D. O. Popa, and S. M. Tousif, "Adaptive admittance control for human-robot interaction using model reference design and adaptive inverse filtering," *IEEE Transactions on Control Systems Technology*, vol. 25, no. 1, pp. 278–285, 2017.
- [21] B. Yao, Z. Zhou, L. Wang, W. Xu, Q. Liu, and A. Liu, "Sensorless and adaptive admittance control of industrial robot in physical human-robot

- interaction,” *Robotics and Computer-Integrated Manufacturing*, vol. 51, pp. 158–168, 2018.
- [22] Y. Li, S. S. Ge, and C. Yang, “Learning impedance control for physical robot–environment interaction,” *International Journal of Control*, vol. 85, no. 2, pp. 182–193, 2012.
- [23] A. Toedtheide, E. Shahriari, and S. Haddadin, “Tank based unified torque/impedance control for a pneumatically actuated antagonistic robot joint,” in *2017 IEEE International Conference on Robotics and Automation (ICRA)*, pp. 1255–1262, IEEE, 2017.
- [24] C. Schindlbeck and S. Haddadin, “Unified passivity-based cartesian force/impedance control for rigid and flexible joint robots via task-energy tanks,” in *2015 IEEE International Conference on Robotics and Automation (ICRA)*, pp. 440–447, IEEE, 2015.
- [25] H. Li, L. Wang, H. Du, and A. Boulkroune, “Adaptive fuzzy backstepping tracking control for strict-feedback systems with input delay,” *IEEE Transactions on Fuzzy Systems*, vol. 25, no. 3, pp. 642–652, 2017.
- [26] X. Chen, C.-Y. Su, Z. Li, and F. Yang, “Design of implementable adaptive control for micro/nano positioning system driven by piezoelectric actuator,” *IEEE Transactions on Industrial Electronics*, vol. 63, no. 10, pp. 6471–6481, 2016.
- [27] Y. Ren, M. Chen, and J. Liu, “Bilateral coordinate boundary adaptive control for a helicopter lifting system with backlash-like hysteresis,” *Science China Information Sciences*, vol. 63, pp. 1–3, 2020.
- [28] C.-B. Yan and Q. Zhao, “Analytical approach to estimate efficiency of series machines in production lines,” *IEEE Transactions on Automation Science and Engineering*, vol. 15, no. 3, pp. 1027–1040, 2018.
- [29] W. He, X. He, and C. Sun, “Vibration control of an industrial moving strip in the presence of input deadzone,” *IEEE Transactions on Industrial Electronics*, vol. 64, no. 6, pp. 4680–4689, 2017.
- [30] W. He and S. S. Ge, “Vibration control of a nonuniform wind turbine tower via disturbance observer,” *IEEE/ASME Transactions on Mechatronics*, vol. 20, no. 1, pp. 237–244, 2015.
- [31] G. Xie, A. Shangguan, R. Fei, W. Ji, W. Ma, and X. Hei, “Motion trajectory prediction based on cnn-lstm sequential model,” *SCIENCE CHINA Information Sciences*, 2020, DOI: 10.1007/s11432-019-2761-y.
- [32] C. Hou and Q. Zhao, “Optimization of web service-based control system for balance between network traffic and delay,” *IEEE Transactions on Automation Science and Engineering*, vol. 15, no. 3, pp. 1152–1162, 2018.
- [33] C. Sun and Y. Xia, “An analysis of a neural dynamical approach to solving optimization problems,” *IEEE Transactions on Automatic Control*, vol. 54, no. 8, pp. 1972–1977, 2009.
- [34] W. He and T. Meng, “Adaptive control of a flexible string system with input hysteresis,” *IEEE Transactions on Control Systems Technology*, vol. 26, no. 2, pp. 693–700, 2018.
- [35] T. Zhao, Y. Liu, Z. Li, C.-Y. Su, and Y. Feng, “Adaptive control and optimization of mobile manipulation subject to input saturation and switching constraints,” *IEEE Transactions on Automation Science and Engineering*, vol. 16, no. 4, pp. 1543–1555, 2018.
- [36] Y. Wu, B. Jiang, and N. Lu, “A descriptor system approach for estimation of incipient faults with application to high-speed railway traction devices,” *IEEE Transactions on Systems, Man, and Cybernetics: Systems*, 2017, DOI: 10.1109/TSMC.2017.2757264.
- [37] G. Xie, L. Sun, T. Wen, X. Hei, and F. Qian, “Adaptive transition probability matrix-based parallel IMM algorithm,” *IEEE Transactions on Systems, Man, and Cybernetics: Systems*, 2019, DOI: 10.1109/TSMC.2019.2922305.
- [38] Y.-J. Liu and S. Tong, “Barrier Lyapunov functions for nussbaum gain adaptive control of full state constrained nonlinear systems,” *Automatica*, vol. 76, pp. 143–152, 2017.
- [39] H. Chen, X. Li, and J. Sun, “Stabilization, controllability and optimal control of boolean networks with impulsive effects and state constraints,” *IEEE Transactions on Automatic Control*, vol. 60, no. 3, pp. 806–811, 2015.
- [40] J. Wu, B. Su, J. Li, X. Zhang, X. Li, and W. Chen, “Adaptive fuzzy control for full states constrained systems with nonstrict-feedback form and unknown nonlinear dead zone,” *Information Sciences*, vol. 376, pp. 233–247, 2017.
- [41] X. Yu, W. He, H. Li, and J. Sun, “Adaptive fuzzy full-state and output feedback control for uncertain robots with output constraint,” *IEEE Transactions on Systems, Man, and Cybernetics: Systems*, 2020, DOI: 10.1109/TSMC.2019.2963072.
- [42] S. Zhang, Y. Dong, Y. Ouyang, Z. Yin, and K. Peng, “Adaptive neural control for robotic manipulators with output constraints and uncertainties,” *IEEE Transactions on Neural Networks and Learning Systems*, vol. 29, no. 11, pp. 5554–5564, 2018.
- [43] K. P. Tee, B. Ren, and S. S. Ge, “Control of nonlinear systems with time-varying output constraints,” *Automatica*, vol. 47, no. 11, pp. 2511–2516, 2011.
- [44] Y.-J. Liu, S. Lu, S. Tong, X. Chen, C. P. Chen, and D.-J. Li, “Adaptive control-based barrier lyapunov functions for a class of stochastic nonlinear systems with full state constraints,” *Automatica*, vol. 87, pp. 83–93, 2018.
- [45] Q. Zhou, L. Wang, C. Wu, H. Li, and H. Du, “Adaptive fuzzy control for nonstrict-feedback systems with input saturation and output constraint,” *IEEE Transactions on Systems, Man, and Cybernetics: Systems*, vol. 47, no. 1, pp. 1–12, 2017.
- [46] Z.-L. Tang, K. P. Tee, and W. He, “Tangent barrier lyapunov functions for the control of output-constrained nonlinear systems,” *IFAC Proceedings Volumes*, vol. 46, no. 20, pp. 449–455, 2013.
- [47] X. Jin, “Fault tolerant finite-time leader–follower formation control for autonomous surface vessels with los range and angle constraints,” *Automatica*, vol. 68, pp. 228–236, 2016.
- [48] D.-P. Li and D.-J. Li, “Adaptive neural tracking control for nonlinear time-delay systems with full state constraints,” *IEEE Transactions on Systems, Man, and Cybernetics: Systems*, vol. 47, no. 7, pp. 1590–1601, 2017.
- [49] Y. Zhang, J. Sun, H. Liang, and H. Li, “Event-triggered adaptive tracking control for multiagent systems with unknown disturbances,” *IEEE Transactions on Cybernetics*, 2018, DOI: 10.1109/TCYB.2018.2869084.
- [50] G. Wu, J. Sun, and J. Chen, “Optimal linear quadratic regulator of switched systems,” *IEEE Transactions on Automatic Control*, vol. 64, no. 7, pp. 2898–2904, 2019.
- [51] C. Sun, W. He, and J. Hong, “Neural network control of a flexible robotic manipulator using the lumped spring-mass model,” *IEEE Transactions on Systems, Man, and Cybernetics: Systems*, vol. 47, no. 8, pp. 1863–1874, 2017.
- [52] M. Chen and G. Tao, “Adaptive fault-tolerant control of uncertain nonlinear large-scale systems with unknown dead zone,” *IEEE Transactions on Cybernetics*, vol. 46, no. 8, pp. 1851–1862, 2016.
- [53] M. Chen, S.-Y. Shao, and B. Jiang, “Adaptive neural control of uncertain nonlinear systems using disturbance observer,” *IEEE Transactions on Cybernetics*, vol. 47, no. 10, pp. 3110–3123, 2017.
- [54] P. Liu, Z. Zeng, and J. Wang, “Multiple Mittag–Leffler stability of fractional-order recurrent neural networks,” *IEEE Transactions on Systems, Man, and Cybernetics: Systems*, vol. 47, no. 8, pp. 2279–2288, 2017.
- [55] A. Wu and Z. Zeng, “Global Mittag–Leffler stabilization of fractional-order memristive neural networks,” *IEEE Transactions on Neural Networks and Learning Systems*, vol. 28, no. 1, pp. 206–217, 2017.
- [56] W. He, S. S. Ge, Y. Li, E. Chew, and Y. S. Ng, “Neural network control of a rehabilitation robot by state and output feedback,” *Journal of Intelligent & Robotic Systems*, vol. 80, no. 1, pp. 15–31, 2015.
- [57] T. Wang, H. Gao, and J. Qiu, “A combined adaptive neural network and nonlinear model predictive control for multirate networked industrial process control,” *IEEE Transactions on Neural Networks and Learning Systems*, vol. 27, no. 2, pp. 416–425, 2016.
- [58] W. He and Y. Dong, “Adaptive fuzzy neural network control for a constrained robot using impedance learning,” *IEEE Transactions on Neural Networks and Learning Systems*, vol. 29, no. 4, pp. 1174–1186, 2018.
- [59] K. J. Hunt, D. Sbarbaro, R. Żbikowski, and P. J. Gawthrop, “Neural networks for control systems: a survey,” *Automatica*, vol. 28, no. 6, pp. 1083–1112, 1992.
- [60] A. Q. Keemink, H. van der Kooij, and A. H. Stienen, “Admittance control for physical human–robot interaction,” *The International Journal of Robotics Research*, vol. 37, no. 11, pp. 1421–1444, 2018.
- [61] S. Zhang, P. Yang, L. Kong, W. Chen, Q. Fu, and K. Peng, “Neural networks-based fault tolerant control of a robot via fast terminal sliding mode,” *IEEE Transactions on Systems, Man, and Cybernetics: Systems*, 2019, DOI: 10.1109/TSMC.2019.2933050.
- [62] K. P. Tee, S. S. Ge, and E. H. Tay, “Barrier Lyapunov functions for the control of output-constrained nonlinear systems,” *Automatica*, vol. 45, no. 4, pp. 918–927, 2009.



**Wei He** (S'09-M'12-SM'16) received the B.Eng. degree in automation and the M.Eng. degree in control science and engineering from the College of Automation Science and Engineering, South China University of Technology, Guangzhou, China, in 2006 and 2008, respectively, and the Ph.D. degree in control science and engineering from the Department of Electrical and Computer Engineering, National University of Singapore, Singapore, in 2011.

He is currently a Full Professor with the School of Automation and Electrical Engineering, University of Science and Technology Beijing, Beijing, China. He has coauthored more than two books in Springer and has authored or coauthored more than 100 international journal and conference papers. His current research interests include robotics, distributed parameter systems, and intelligent control systems.

Prof. He was a recipient of the Newton Advanced Fellowship from the Royal Society, U.K., in 2017 and the IEEE SMC Society Andrew P. Sage Best Transactions Paper Award in 2017. Since 2018, he has been the Founding Chair of the Technical Committee on Autonomous Bionic Robotic Aircraft (TC-ABRA), IEEE Systems, Man and Cybernetics Society. He is serving as the Chair for the IEEE SMC Society Beijing Capital Region Chapter. He is also serving as an Associate Editor for the *IEEE Transactions on Robotics*, *IEEE Transactions on Neural Networks and Learning Systems*, *IEEE Transactions on Control Systems Technology*, *IEEE Transactions on Systems, Man, and Cybernetics: Systems*, *SCIENCE CHINA Information Sciences*, *IEEE/CAA Journal of Automatica Sinica*, *Neurocomputing*, and an Editor for the *Journal of Intelligent and Robotic Systems*.



**Chenguang Yang** (M'10-SM'16) received the Ph.D. degree in control engineering from the National University of Singapore, Singapore, in 2010.

He is a Professor of Robotics with Bristol Robotics Laboratory, University of the West of England, Bristol, U.K. His current research interests include human-robot interaction and intelligent system design.

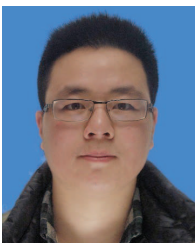
Prof. Yang has been awarded the EU Marie Curie International Incoming Fellowship, U.K. EPSRC UKRI Innovation Fellowship, and the Best Paper

Award of the *IEEE Transactions on Robotics* as well as over ten conference best paper awards.



**Chengqian Xue** received the B.E. degree in automation (Excellence Program) from the School of Advanced Engineering, University of Science and Technology Beijing, Beijing, China, in 2018, he is currently pursuing the M.E. degree in control science and engineering from the School of Automation and Electrical Engineering, University of Science and Technology Beijing, Beijing, China.

His current research interests include adaptive neural networks control, robotics and human-robot interaction.



**Xinbo Yu** (S'16) received the B.E. degree in control technology and instrument from the School of Automation and Electrical Engineering, University of Science and Technology Beijing, Beijing, China, in 2013, where he is currently pursuing the Ph.D. degree in control theory and control engineering.

His current research interests include adaptive neural networks control, robotics and human-robot interaction.



**Zhijun Li** (M'07-SM'09) received the Ph.D. degree in mechatronics, Shanghai Jiao Tong University, P. R. China, in 2002. From 2003 to 2005, he was a postdoctoral fellow in Department of Mechanical Engineering and Intelligent systems, The University of Electro-Communications, Tokyo, Japan. From 2005 to 2006, he was a research fellow in the Department of Electrical and Computer Engineering, National University of Singapore, and Nanyang Technological University, Singapore. From 2017,

he is a Professor in Department of Automation, University of Science and Technology, Hefei, China. From 2019, he is the Vice Dean of School of Information Science and Technology, University of Science and Technology of China, China.

From 2016, he has been the Co-Chairs of IEEE SMC Technical Committee on Bio-mechatronics and Bio-robotics Systems (*B<sup>2</sup>S*), and IEEE RAS Technical Committee on Neuro-Robotics Systems. He is serving as an Editor-at-large of *Journal of Intelligent and Robotic Systems*, and Associate Editors of several *IEEE Transactions*. Dr. Li's current research interests include wearable robotics, tele-operation systems, nonlinear control, neural network optimization, etc.